On the divergence of the auroral electrojets

Octav Marghitu[1], Costel Bunescu[1], Tomas Karlsson[2], Berndt Klecker[3], and Hans C. Stenbaek-Nielsen[4]

Abstract. The current configuration in the auroral region is known to consist typically of downward and upward field-aligned current (FAC) sheets, connected in the ionosphere by meridional Pedersen currents, while divergence free electrojets (EJs) flow azimuthally as Hall currents. This configuration of the auroral current circuit was introduced by *Boström* [1964] and labelled as 'Type 2', while he suggested also an alternative 'Type 1' configuration, with filamentary FACs connected in the ionosphere by azimuthal Pedersen currents. By using an updated version of the recently developed ALADYN technique, we investigated the divergence of the auroral electrojets for a few FAST crossings over the auroral oval in the 20–22 MLT sector, two of which are presented in detail. Although a precise estimate of the electrojet divergence is difficult, because of several error sources, the results suggest that this divergence can be significant over certain latitude ranges, comparable with the FAC density. Direct FAC–EJ coupling appears to contribute to the ionospheric current closure not only during active times, as already known, but also during rather quiet periods. The quiet time FAC–EJ coupling is likely to be achieved in a mixed 'Type 1/Type 2' configuration, with the FAC sheet (Type 1) azimuthally connected to the Pedersen component of the EJ (Type 2). This configuration requires a non-zero tangential component of the electric field, and is therefore more likely realized inside or near the Harang region. At the same time, the divergence of the Hall current is presumably negligible, and likewise the ionospheric polarization, consistent with statistical results published recently. During more active intervals and possible reconfigurations of the auroral current circuit, our results suggest that the FAC–EJ coupling could be also achieved by Hall currents. We conclude by exploring a tentative scenario for the integrated evolution of the ionospheric current closure and Cowling mechanism during the substorm cycle. A systematic examination of more experimental evidence is needed to validate this scenario.

1. Introduction

Auroral arcs are typically described in terms of 1D stripes of increased ionospheric conductance. An upward field-aligned current (FAC) sheet above the arc is connected by Pedersen current to a downward FAC sheet near the arc, while a divergence free Hall current electrojet (EJ) flows along the arc (Fig. 1a). In this simplest case, both the Pedersen and Hall currents are driven by an electric field normal to the arc. The 1D arc model, including sometimes a (fairly small) tangential electric field, is often realized in the evening and morning sectors of the auroral oval, and was studied extensively in the past, based on radar, rocket, and satellite data [e. g. *de la Beaujardière et al.*, 1977; *Marklund*, 1984; *Sugiura*, 1984]. The 1D arc behaves as a partial Cowling channel, with current continuity achieved by FAC and ionospheric polarization. The relative proportion of the two depends on the local efficiency of the Cowling mechanism, discussed most recently by *Amm et al.* [2011] and *Fujii et al.* [2011].

A similar configuration is realized also on oval scale, where downward and upward (thick) FAC sheets are connected meridionally by Pedersen currents, driven by meridional electric fields. Following *Iijima and Potemra* [1976], the poleward and equatorward FAC sheets are called, respectively, Region 1 (R1) and Region 2 (R2) currents. In the evening sector the downward R2 current feeds an upward R1 current, and the meridional electric field points poleward, while in the morning sector the electric field points equatorward and the sense of the two FACs is reversed. The meridional electric field drives an eastward electrojet (EEJ) in the evening sector and a westward electrojet (WEJ) in the morning sector. For the electric field and current configuration on oval scale the reader is referred e. g. to the review by *Baumjohann* [1982]. The overlap region of the evening and morning sectors, before and around midnight, is called the Harang region (HR). In the HR, the electric field rotates from poleward to westward and finally to equatorward, while the EEJ and WEJ are both present, shifted in latitude, on a given meridian.

In contrast to the 1D model, real arcs can exhibit also 2D features: the FAC can close not only normal to the arc but also along the arc, via both Pedersen and Hall currents, while the electric field can have a significant component along the arc (Fig. 1b). By using FAST data and the newly developed ALADYN technique [*Marghitu et al.*, 2004, 2009], one can derive the full set of electrodynamic quantities along the ionospheric satellite footpoint (Pedersen and Hall conductance, the two components of the electric field, field-aligned and ionospheric current) and explore locally the 3D current closure. In these two papers, referred in the following as M04 and M09, the electrojets were no longer assumed divergence free, and average values of the divergence over certain intervals were derived based on the measured data.

[1]Institute for Space Sciences, Bucharest, Romania.
[2]Space and Plasma Physics, Royal Institute of Technology, Stockholm, Sweden.
[3]Max Planck Institute for Extraterrestrial Physics, Garching, Germany.
[4]University of Alaska at Fairbanks, Fairbanks, USA.

0148-0227/11/$9.00

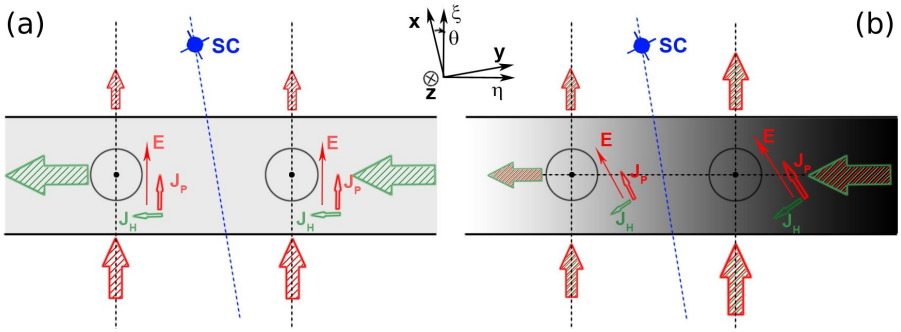

Figure 1. 1D (a) and 2D (b) arc models. The conductance, FAC, ionospheric electric field, and ionospheric current are indicated by the gray shade, circles, solid arrows, and hatched arrows respectively. Red and green show the Pedersen and Hall components of the current. The spacecraft trajectory is indicated as well. For the 1D model, the FAC is closed by Pedersen current, driven by electric field normal to the arc. The electric field drives as well a divergence free Hall current electrojet. For the 2D model the FAC is fed by both normal and longitudinal (electrojet) currents, both including a Pedersen and a Hall component, due to the tilted electric field. The divergence of the electrojet can be related to variations in the electric field and / or conductance. The reference frames associated with the arc (ξ, η) and satellite footpoint (x, y), are indicated as well. The angle θ between the two systems is typically small for satellites on polar orbits.

As suggested by M09, the electric field and current configuration in the HR is particularly suited for 2D effects, on both arc and oval scale. A closer investigation of the arcs inside and nearby to the HR may help to a better understanding of both arc electrodynamics and substorm physics. The auroral activity in the HR [e. g. *Nielsen and Greenwald*, 1979; *Zou et al.*, 2009] is thought to be closely related to the substorm onset, but the details of this relationship are not fully understood [*Weygand et al.*, 2008]. While meso-scale investigations of HR electrodynamics are possible based on ground data [e. g *Amm et al.*, 2000], high-resolution satellite data are required for the smaller scale arc studies.

The goal of this paper is threefold: *i) First*, to develop the ALADYN technique further, in order to investigate the electrojet divergence on a 'continuous' basis, not just for certain intervals, as done before. *ii) Second*, to check the updated technique on two events, infer the electrojet divergence, and compare it with the FAC density. *iii) Third*, to explore the M–I coupling implications of the ionospheric current closure. While some of the ideas below were introduced in M04 and developed in M09, the approach proposed here allows for a more systematic evaluation of the data and extends the examination of the M–I coupling implications. In Section 2, we briefly summarize the ALADYN technique and introduce its new features. The ALADYN results for two FAST events and a discussion of possible error sources are presented in Section 3. M–I coupling implications of the ionospheric current closure are examined in Section 4 and a concise summary concludes the paper in Section 5.

2. The ALADYN method: Summary and update

The ALADYN method enables a realistic description of auroral electrodynamics, on both arc and oval scales. ALADYN relies on current continuity at ionospheric level and on a parametric model that includes the tangential electric field and the divergence of the electrojet. In arc coordinates (see Fig. 1), the 1D current continuity writes:

$$j_{\parallel} - \frac{dJ_{\xi}}{d\xi} = 0 \tag{1}$$

or, expressing the FAC density, $j_{\parallel}$, by Ampére's law:

$$\frac{d}{d\xi}(H_{\eta} - J_{\xi}) = 0 \tag{2}$$

This equation integrates to:

$$H_{\eta} - J_{\xi} = c_0 \tag{3}$$

where H_{η} is the integrated FAC fed to the ionosphere, J_{ξ} is the ionospheric meridional current, and c_0 is the constant difference of the two. One simple step towards a 2D arc model is to allow a finite but constant (in normal direction) divergence of the electrojet, $\partial J_{\eta}/\partial\eta = c_1$. In this case the current continuity Eq. (1) becomes:

$$j_{\parallel} - \frac{\partial J_{\xi}}{\partial \xi} = \frac{\partial J_{\eta}}{\partial \eta} = c_1 \tag{4}$$

which can be integrated, as before, along ξ, yielding:

$$H_{\eta} - J_{\xi} = c_0 + c_1\xi \tag{5}$$

Strictly speaking, in Eq. (5) c_0 and c_1 can depend on η, but this dependence can be neglected if the satellite crossing is normal to the arc / oval, or close to normal (that is, if the satellite displacement in longitudinal direction is small compared to the length scale of the electrojet).

By using Ohm's law to replace J_{ξ} (with Σ_P and Σ_H the Pedersen and Hall conductance, respectively), by assuming that the electric field is uniform in η direction, which implies (via Faraday's law) that E_{η} is constant, $E_{\eta} = b_0$, and by expressing E_x as the sum of the measured average electric field (E_{0_x}) plus an unknown expansion in Legendre polynomials (G_i), $E_x = E_{0_x} + \sum_{i=1}^{n_x} a_i G_i$, Eq. (5) can be cast into the fit equation:

$$\frac{\Sigma_P}{\cos\theta}\sum_{i=1}^{n_x} a_i G_i - (\Sigma_H - \Sigma_P \tan\theta)b_0 + c_0 + c_1 x\cos\theta = H_y\cos\theta - H_x\sin\theta - \frac{\Sigma_P E_{0_x}}{\cos\theta} \tag{6}$$

used to derive the parameters (a_i, b_0, c_0, c_1). As discussed below, if the tangential electric, b_0, and the electrojet divergence, c_1, are fixed, Eq. (6) provides an approximation of the unique E_x solution and unique c_0 constant. The higher is the order, n_x, of the series expansion, the better is the approximation. In practice, n_x depends on the conductance profile and larger values are needed when the conductance variability is higher (within the limit imposed by data resolution).

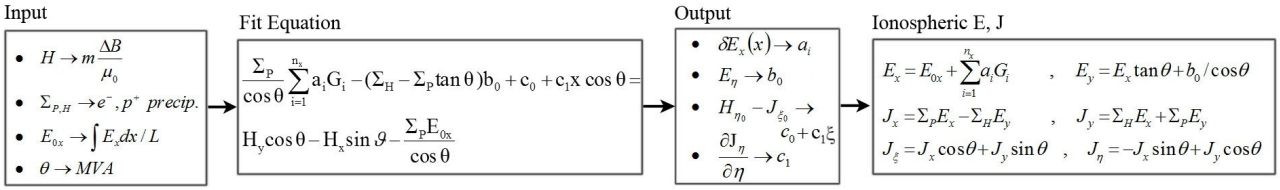

Figure 2. The logic of the ALADYN method, as introduced in M04 and M09, from the input data to the ionospheric electric field and current, via the fit equation and the output parameters. The 'Input' box shows the relation of the input quantities to the measured data, while the 'Output' box indicates the significance of the output parameters. The ionospheric electric field and current are finally derived by using the fitted parameters, as presented in the 'Ionospheric E, J' box. Note that the updated ALADYN does not derive c_1 directly, by fit, any more, but indirectly, from the variation of c_0 (see text).

The required input quantities are obtained from the measured magnetic field, electric field, and particle data. Figure 2 shows the logic of the ALADYN method, as introduced in M04 and M09, from the input data to the ionospheric electric field and current (the updated ALADYN does not derive c_1 directly, by fit, any more, but indirectly, from the variation of c_0). The events of interest are assumed to map onto the dark auroral oval, where the conductance is mainly induced by particle precipitation. Estimates of the electron and proton terms, Σ^e and Σ^p, are derived according to *Robinson et al.* [1987] and *Galand and Richmond* [2001], respectively:

$$\Sigma_P^e = \frac{40\overline{E}}{16+\overline{E}^2}\Phi_E^{1/2} \qquad \Sigma_P^p = 5.7\Phi_E^{1/2} \quad (7)$$

$$\frac{\Sigma_H^e}{\Sigma_P^e} = 0.45\overline{E}^{0.85} \qquad \frac{\Sigma_H^p}{\Sigma_P^p} = 0.45\overline{E}^{0.3} \quad (8)$$

where Φ_E is the energy flux in mW/m^2 and $\overline{E}$ is the average energy in keV, $\overline{E} = \Phi_E/\Phi_N$, with Φ_N the number flux. 'P' and 'H' stand for 'Pedersen' and 'Hall'. The total conductance is obtained by:

$$\Sigma_{P,H} = \sqrt{\Sigma_{P,H}^{e^2} + \Sigma_{P,H}^{p^2}} \quad (9)$$

The ALADYN method allows the cross-check of the results by three different consistency tests. First, the ionospheric electric field should be equal to the mapped field measured by FAST as long as the field-aligned potential drop below the satellite is zero (that is, as long as ion beams are not observed). Second, if ALADYN is applied on adjacent sub-intervals (e.g. Region 1 and Region 2 FAC), a good overall electric field solution should be continuous at the edges of the sub-intervals, except for cases when polarization charge can support a locally divergent electric field. Third, according to Eq. (5), $H_{\eta_0} - J_{\xi_0}$ should be constant if the electrojet is divergence free, $c_1 = 0$, namely the c_0 parameter derived by fit should be constant. Under the assumption of a divergence free electrojet, all the current fed by the FAC, measured by H_η, can only be continued by J_ξ, in normal / meridional direction. If the background current between the sub-auroral region and the polar cap is negligible, c_0 should be equal to 0. While M04 and M09 made use of the first and second consistency tests, here we shall continue to use the first test but replace the second test by the third test, in a 'continuous' formulation of ALADYN. The variation of c_0, computed over a sliding window along the investigated interval, will be used to estimate the electrojet divergence.

When the electrojet divergence, c_1, is fixed (including the case when it is zero), the electric field solution of Eq. 4 is unique, for a given FAC density, $j_\parallel$, a given tangential electric field, b_0, and a given average electric field, E_{0_x}. Indeed, with $J_\xi = \Sigma_P E_\xi - \Sigma_H b_0$, Eq. 4 can be re-written as a first order differential equation in E_ξ:

$$\Sigma_P \frac{dE_\xi}{d\xi} + \frac{d\Sigma_P}{d\xi} E_\xi = j_\parallel + b_0 \frac{d\Sigma_H}{d\xi} - c_1 \quad (10)$$

Incidentally, the l.h.s. of Eq. (10) shows the divergence of the normal Pedersen current, which is fed by the FAC, the divergence of the normal Hall current, and the divergence of the electrojet (first, second, and third right term, respectively). If all the right terms are known, the solution of Eq. (10) is unique, once the value of E_ξ at a certain point ξ_0 is fixed. Since Eq. (6) is the integral form of Eq. (10), fixing E_ξ at a certain point is equivalent to fixing the integration constant, c_0. Because of its specific formulation, with E_x developed in a series expansion, ALADYN uses a fixed average electric field, instead of a fixed electric field at a certain point. This is also more robust from a data perspective, since the error of the average is smaller than the error of a particular value.

The fit equation (6) can be solved assuming a divergence free electrojet, $c_1 = 0$, for a set of different b_0 values, over a sliding window to be moved at a certain time step. For each b_0 one obtains thus a series of fitted electric field solutions, E_x^f (one solution extending over the sliding window at a certain time step), that can be compared with the mapped measured electric field, E_x^m. Specifically, we shall compute the quantity δE_x, defined as:

$$\delta E_x = \sqrt{\sum_{i=1}^{n} (E_{x_i}^f - E_{x_i}^m)^2/n)} \quad (11)$$

where n is the number of data points in the window. One also obtains a series of c_0 values, that can be used to check the divergence of the electrojet, c_1, depending as well on b_0. In this formulation of ALADYN c_1 is no longer obtained directly by fit, as in M04 and M09, but inferred from the variation of c_0, namely $c_1 = \Delta c_0/\Delta x \cos\theta$. A positive / negative variation of c_0 indicates a positive / negative divergence of the electrojet. In order to find the most likely range for the actual value of b_0, the updated ALADYN relies as well on the two sets of profiles, δE_x and c_0.

3. FAST observations and ALADYN results

While the ALADYN method takes into account 2D arc (and oval) features, the assumptions made still require the elongated arc geometry. Since time dependent effects are not included in the fit equation (6), ALADYN also requires a rather stationary configuration over the fit window, therefore the width of this window should be small compared to the time scale of the auroral activity. The geometry and dynamics of the aurora can be best judged from conjugate optical data. When optical data are not available, ground

magnetic data can be used to get information on the dynamics, while the *in-situ* magnetic perturbation enable the check of the arc geometry.

In the following we shall examine in detail two conjugate events, FAST orbits 1859 and 1805. The first event, already investigated in M04 and M09, will be re-visited in order to validate the new ALADYN features. The second event was selected from two optical campaigns conjugate with FAST, carried on in January–February 1997 and 1998 by the Geophysical Institute at the University of Alaska, Fairbanks. Details on these two campaigns can be found in *Stenbaek-Nielsen et al.* [1998] and in the Data → Conjunctive Studies section of the FAST mission site. All the 29 events of these campaigns were located at 20–22 MLT, presumably many of them inside or nearby the HR, providing thus a promising database for future investigations.

3.1. Event 1: FAST Orbit 1859

Figure 3 summarizes the relevant optical and FAST data for the first event, in the top and middle panels, as well as the results of the ALADYN processing in the two bottom panels. Details on the FAST, optical, and geophysical background data, observed during the growth phase of asmall substorm, are presented in M09. As compared to M09, the time interval explored here is a bit longer, 8:19:00–8:23:20 UT, fully encompassing the FAC region (Fig. 3e), and the electric potential along the FAST footpoint (Fig. 3d) is corrected for corotation. As discussed already in M04, the corotation correction does not change the important feature that the minimum potential is reached at 8:22:04 — therefore the electric field / plasma convection reversal (CR) is located well within the FAC region and close to the FAC reversal (FR) from downward to upward. However, the corotation correction is important for Event 2, prompting a similar treatment for Event 1. As compared to M09, the ionospheric potential is also extended, by linear interpolation, over ion beam intervals (when the electric field measured by FAST cannot be mapped to the ionosphere) and over intervals of unreliable electric field data (e. g. due to high satellite potential in the low density plasma of the auroral acceleration region).

The two bottom panels of Fig. 3 reflect the update of the ALADYN technique, as introduced in Section 2, by showing δE_x and the fit parameter c_0 depending on b_0. The results were obtained with a sliding window of 15 s moved in steps of 1 s (similar results were obtained for windows of 10 and 20 s). Each plot shows a total of 13 lines, with b_0 in the range [-40, 20] mV/m, varied in steps of 5 mV/m. The actual value of the tangential electric field, which is typically zero or slightly negative, is presumably included in this range. Apriori, when varying b_0 from -40 mV/m to 20 mV/m, i.e. from a large westward to a moderate eastward field, one expects to see a minimum in δE_x corresponding to the actual value of b_0 (a perfect match between the fitted and measured electric field would imply a minimum δE_x equal to zero, but in practice this is unlikely to happen).

In Fig. 3f the dependence of δE_x on b_0 has the expected behavior over the periods around 8:22:10 and 8:22:25. At these times Σ_H is substantial, up to 28 mho at 8:22:12, and has large gradients, enabling the normal Hall current, $J_{\xi_H} = \Sigma_H b_0$, to contribute to the current closure. In between these times, around 8:22:20, there is little dependence of δE_x on b_0, because of the plateau in the Hall conductance, $\Sigma_H \simeq 10$ mho, yielding a constant J_{ξ_H} that does not contribute to the current closure. Consequently, E_x^f and further δE_x depend only weakly on b_0. The same weak dependence on b_0 is seen also over the low conductance regions before 8:21:00 and after 8:22:40. Because of the small Σ_H, the contribution of J_{ξ_H} to the current closure is small as

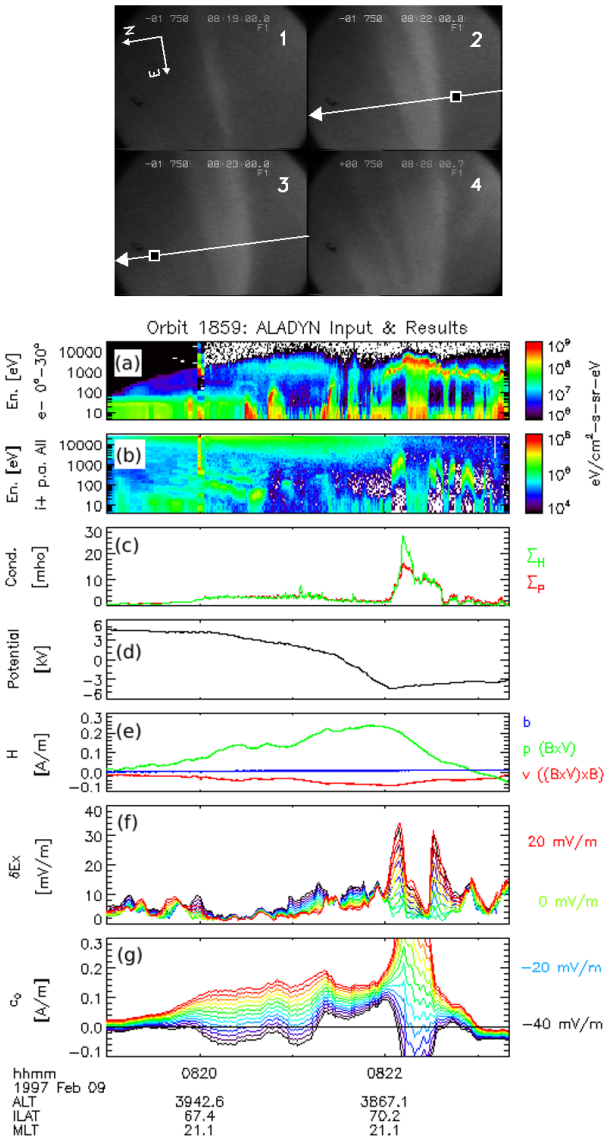

Figure 3. *Top:* Ground optical data conjugate with FAST overpass. The four frames show a stationary arc during the ∼1 min FAST overpass, but a gradual development on a ∼10 min time scale. *Middle:* FAST data. (a) Electron and (b) ion time–energy spectrograms; (c) Pedersen and Hall conductance; (d) ionospheric potential along the FAST footpoint; (e) magnetic field perturbation. *Bottom:* ALADYN results. (f) Difference, δE_x, between the fitted ionospheric electric field and the measured electric field mapped to the ionosphere, computed according to Eq. (11) and depending on the tangential electric field, b_0; (g) integration constant c_0, depending as well on b_0. The b_0 step between two consecutive lines is 5 mV/m, within the range [-40, 20] mV/m.

well, and δE_x is barely sensitive to the change in b_0. On the other hand, in these regions the variability of δE_x along the satellite footpoint is probably related to the errors in conductance, compensated by errors in E_x^f.

Between 8:21:00 and 8:22:00 one can identify two regions where the smallest δE_x is obtained for the largest positive b_0 (the red lines near the bottom of the plot). This feature, to be observed also for Event 2, can be explained as follows: Because of the low electron precipitation, the conductance profile is seen to be more noisy in these regions. As long

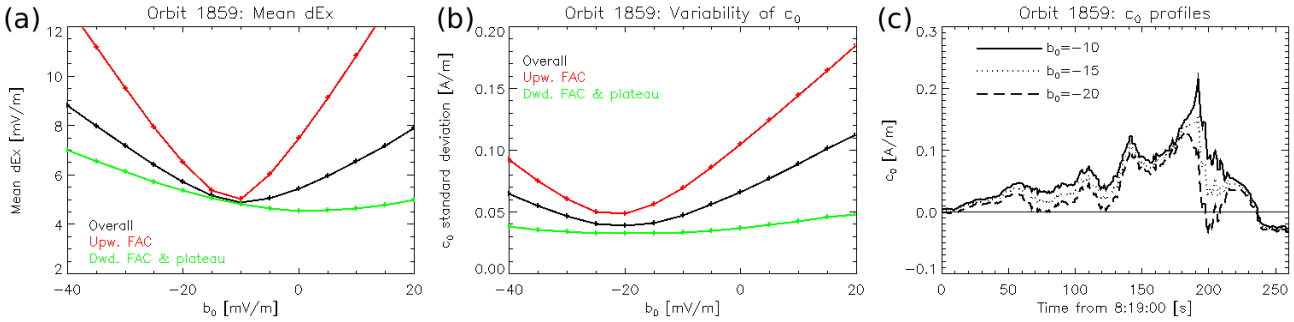

Figure 4. *(a), (b):* Mean δE_x and Σ_{c_0}, the standard deviation of c_0, as functions of the tangential electric field, b_0. The black, red, and green lines show results for the whole FAC region, upward FAC, and downward FAC, respectively. *(c):* The c_0 profile for $b_0 = -20$, -15, and -10 mV/m.

as b_0 is negative (westward), J_{ξ_H} is poleward, same as J_{ξ_P} driven by the poleward average field, E_{0_x}. Since Σ_P and Σ_H are roughly equal, the noisy changes in J_{ξ_H} can be compensated by changes in J_{ξ_P} only for rather large variations of E_x^f around E_{0_x}. Because in these regions E_x^m is rather constant over the width of the sliding window, and therefore essentially equal to E_{0_x}, the variations in E_x^f are reflected by a larger δE_x. When b_0 becomes positive (eastward), J_{ξ_H} is equatorward, opposite to J_{ξ_P}, therefore at comparable noise fluctuations of Σ_P and Σ_H the two components of the current vary in opposite directions, and compensate each other without large variations in E_x. Consequently, δE_x minimizes for the largest positive b_0, as indicated by Fig. 3f.

The c_0 profiles in Fig. 3g allow a rough evaluation of the assumption that the electrojet is divergence free. If this assumption holds, one should find that c_0 is essentially constant for a certain b_0, presumably a b_0 around the value that minimizes δE_x. In reality, a certain variability is always present in c_0, not only for the extreme, black ($b_0 = -40$ mV/m) and red ($b_0 = 20$ mV/m) lines, but also for the cyan–green lines in the middle of the plot (b_0 from -20 to 0 mV/m). According to Eq. (3), this means that $H_\eta - J_\xi$ varies along the satellite footpoint, contradicting the assumption that the electrojet is divergence free. The variation of c_0 is in the range of 0.1–0.2 A/m, of the same order as the integrated sheet FAC, and therefore significant.

Based on the variation of c_0, the electrojet has, on average, a positive divergence from about 8:21:00–8:22:00, and a negative divergence from about 8:22:00–8:23:00, consistent with M09. Before 8:21:00, c_0 is rather flat, but its value is seen to depend on b_0. The flat c_0 indicates that the assumption of a divergence free electrojet is consistent in this region, and the FAC closure is achieved based on the gradual increase of the poleward E_x, resulting in the increase of J_{ξ_P}. On the other hand, since J_{ξ_H} has little variation along the satellite footpoint in this region, not contributing to the current closure, its modification due to the change in b_0 is compensated by the change in c_0. This change becomes significant (and the lines in Fig. 3g better separated) only when the conductance raises from the background level to a few mho, due to proton precipitation at the equatorward side of the downward FAC region.

The dependence of the fit quality and c_0 variability on b_0, as well as the c_0 profile for three more likely b_0 values, can be examined closer in Fig. 4. The mean δE_x in Fig. 4a is computed for each line of Fig. 3f, and the standard deviation of c_0 in Fig. 4b, σ_{c_0}, for each line of Fig. 3g. In both cases we show three results, over the downward and plateau, upward, and whole FAC region. The three profiles in Fig. 4c correspond to b_0 between -20 and -10 mV/m, the values where σ_{c_0} and δE_x reach their respective minima. Note that the b_0 value inferred in M09, of around -12 mV/m, is included in this range.

Figure 4a indicates that the best E_x fit is obtained for $b_0 \simeq -10$ mV/m. The mean δE_x is quite sensitive to b_0 over the large scale upward FAC, and therefore also over the whole FAC region. Some sensitivity is seen also over the large scale downward FAC, but in this case the location of the minimum mean δE_x at $b_0 \simeq 0$ is less reliable, considering the weak dependence of δE_x on b_0 and the larger errors in conductance, discussed above. The positive (instead of zero) value of the minimum mean δE_x, could be, to some extent, the effect of neglecting the divergence of the electrojets, which contributes to an imperfect fit. The variability of c_0 in Fig. 4b, whose minimum standard deviation is around 0.05 A/m, is also consistent with a non-zero divergence of the electrojets. Again, the variability of c_0 is barely sensitive to b_0 over the downward FAC, but rather sensitive over the upward FAC, for example $\sigma_{c_0} = 0.07$ A/m at $b_0 = -10$ mV/m, 40 % larger than the minimum value.

The profile of c_0 in Fig. 4c allows a quantitative examination of the electrojet divergence. For the solid line, corresponding to the best fit (minimum δEx), from 8:21:00 to 8:22:04 (CR) the EEJ has an average positive divergence of about 0.1 A/m / 180 km, that is some 0.6 μA/m^2. This value compares quite well with 0.4 μA/m^2, inferred in M09 for the time interval 8:20:30–8:22:04, providing about the same integrated current. The divergence continues to be positive a few seconds beyond the CR, indicating that the meridional current feeds both the upward FAC and the WEJ — again consistent with M09. While at the CR, the meridional current consists (by definition) of poleward Hall current, shortly afterward (as indicated by the sharpness of the potential change in Fig. 3d), the equatorward Pedersen current becomes comparable to the Hall current. Except for the very close neighborhood of the CR, the meridional current is quite small, but its exact value and sign are difficult to find, due to the uncertainty in b_0. Later on, when Σ_H peaks, from about 8:22:10–8:22:20, c_0 decreases abruptly about 0.1 A/m. This value is comparable to the decrease of the FAC H_p in Fig. 3e over the same interval, and corresponds to a current density of about 3.3 μA/m^2. At this time $\Sigma_P \simeq 15$ mho (Fig. 3c) and with $E_\eta \simeq -10$ mV/m one obtains a Pedersen component of the westward tangential current $J_{\eta P} \simeq 0.15$ A/m. If the EJ divergence were achieved only at the expense of the Pedersen current, its variation length scale should be roughly equal to 0.15 A/m / 3.3 μA/m^2, that is some 50 km. This length appears to be quite short and suggests that the Hall component of the EJ contributes as well to the FAC closure, a point to be discussed further in Section 4.1.

The average electrojet divergence over the time interval 8:22:04–8:23:00 is about -0.2 A/m / 160 km, that is some -1.3 μA/m^2, to be compared with -1.5 μA/m^2 inferred in M09. Figure 4c shows also that a rather small change in b_0 can be associated with a significant change in the small scale current structure in the high conductance region. However, when averaged over the large scale, dominated by rather low conductance, the change is less significant.

To summarize, the application of the updated ALADYN technique to FAST orbit 1859 provided results consistent with M09, and enabled in addition a more detailed exploration of the electrojet divergence.

3.2. Event 2: FAST Orbit 1805

Optical and FAST data for Orbit 1805 are presented in Fig. 5. As indicated by the ground magnetic field (not shown), the observations were made during a quiet interval. The frames at the top of the figure, 1 min apart, show a rather stable double arc, as well as a third arc, that gradually vanishes over the 3 min between frame 1 and frame 4 (frame 1 appears rotated as compared to the other frames because of an aircraft maneuver). Similar, to some extent, to Event 1, the aurora appears to be stable along the satellite footpoint from 8:29–8:30, when FAST crosses above the double arc, but some variation is visible on a longer, few minutes time scale. The electron precipitation, Fig. 5a, and the conductance profile, Fig. 5c, reflect as well the double arc structure, underlined by the large scale upward FAC, Fig. 5e, from 8:29:00–8:30:20. The electric potential, Fig. 5d, reaches its minimum beyond the poleward boundary of the FAC region, around 8:31:00 (not shown), but the slope of the potential indicates a sharp decrease in the electric field around 8:29:00, at the equatorward edge of the large scale upward FAC. In this case the corotation correction is essential for the proper location of the potential minimum and CR boundary.

The data for Event 2 suggest, at first glance, a standard, Boström Type 2 configuration. The downward current until 8:28:00 appears to feed a poleward Pedersen current, under roughly constant conductance conditions, therefore the electric field — and the slope of the potential — gradually increases. Note that in Fig. 5c the conductance is computed only based on proton precipitation until 8:28:45, since the electron precipitation is too weak and noisy. The current fed by the downward FAC keeps flowing, apparently as Pedersen current, until 8:29:00, and the slight increase in the electric field after 8:28:30 (visible as a slight steepening in the potential) is associated with the decrease in proton precipitation and conductance. After 8:29:00 the Pedersen current feeds the upward FAC, back to the magnetosphere, closing thus the Type 2 circuit. Over the upward FAC region the conductance is higher and the electric field required to carry the current is smaller than before, explaining thus the change in the potential slope at 8:29:00.

While the brief examination of the data above appears to indicate a typical evening oval and typical auroral arcs, the application of ALADYN, Figs. 5f and 5g, suggests a more complex picture. Figure 5f exhibits similar features with those observed for Event 1. Over the upward FAC region, where the conductance is high, δE_x minimizes for b_0 around zero. When the conductance is low and mostly smooth, before 8:28:45 and after 8:30:10, δE_x is not very sensitive to b_0. From 8:28:45–8:29:00, where the conductance is low and noisy (because of the electron contribution), the smallest δE_x is obtained for $b_0 = 20$ mV/m, the largest eastward tangential field. Contrary to the expectations based on the Type 2 configuration, Fig. 5g suggests that the electrojet divergence is significant also in this case, with variations in c_0 of up to ∼0.2 A/m, again comparable with the total FAC sheet current.

As before, a better view over the fit accuracy — as expressed by the mean δE_x —, over the variability of c_0, and over three c_0 profiles is provided by Fig. 6. This time the best fit is obtained for b_0 between -5 and 0 mV/m, where the black line in Fig. 6a reaches a flat minimum, while σ_{c_0} in Fig. 6b minimizes for b_0 between -5 and -10 mV/m. Like for Event 1, the dependence of the mean δE_x and of σ_{c_0} on

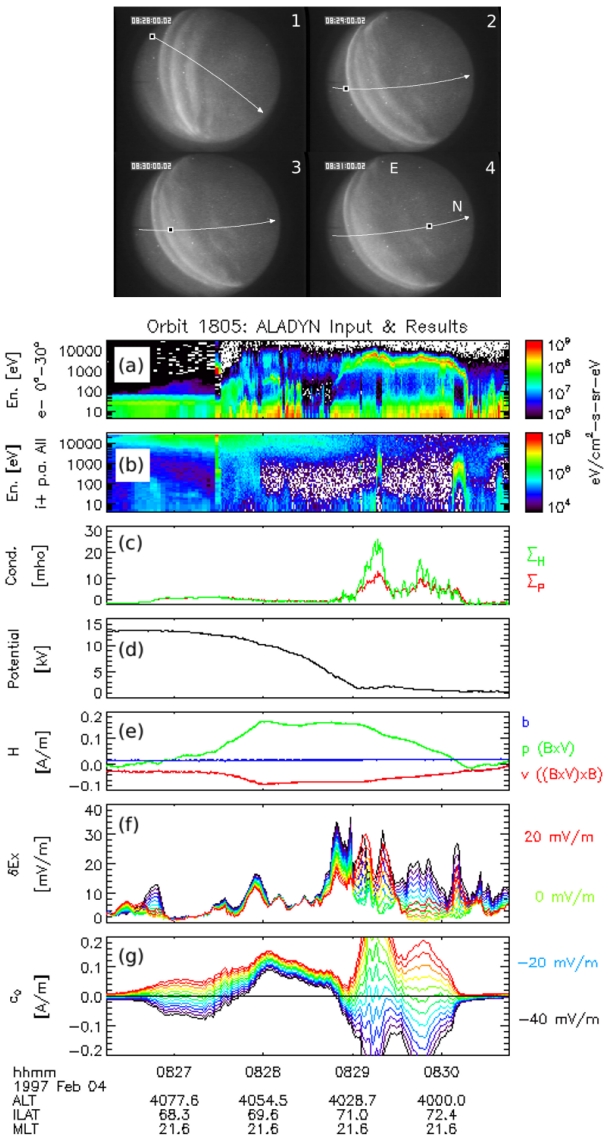

Figure 5. *Top:* Optical data by an aircraft borne all-sky camera, conjugate with FAST overpass. The four frames are 1 min apart, with FAST crossing over the double arc structure between frames 2 and 3. The North and East direction for frames 2–4 are indicated in frame 4. Frames 2–4 are rotated with respect to frame 1 because of an aircraft maneuver. *Middle* and *Bottom*: FAST data and ALADYN results, same layout as in Fig. 3.

b_0 is more pronounced over the upward FAC region, where J_{ξ_H} has substantial variations and makes a significant contribution to the current closure.

Turning to the c_0 profiles in Fig. 6c, until 8:28:00 c_0 raises from 0 to more than 0.1 A/m, that is more than half of the downward FAC, which appears thus to feed the EEJ. Further on, over the region with no FAC, 8:28:00–8:29:00, c_0 returns to 0, which means that the EEJ there feeds the poleward ionospheric current. Overall, the ionospheric current that enters the upward FAC region is equal to the current supplied to the ionosphere by the downward FAC (that is $\gtrsim$0.15 A/m), as for the Type 2 configuration, but the detailed current flow appears to be more complicated. The same is seen over the upward FAC region, where the main feature of c_0 is a steep increase from 8:29:00–8:29:15, followed by a steep decrease until 8:29:30 or later, depending

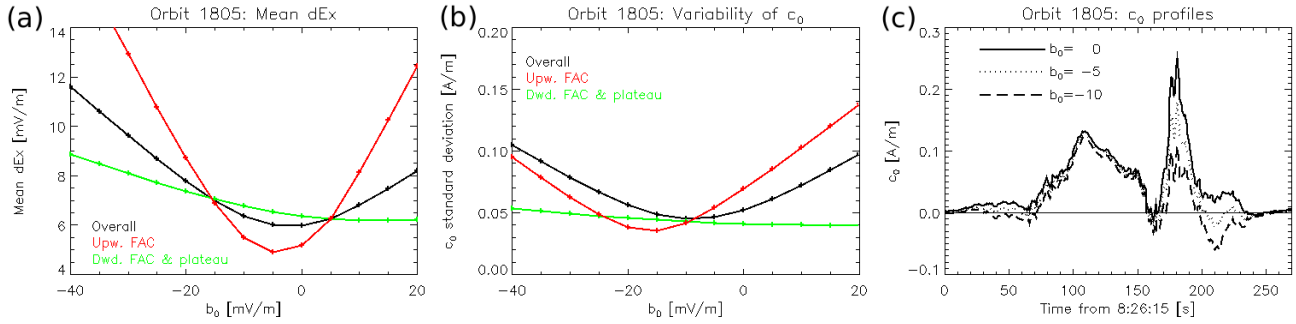

Figure 6. Mean δE_x, σ_{c_0}, and c_0 profiles for $b_0 = -10$, -5, and 0 mV/m. Same layout as in Fig. 4.

on the profile. For $b_0 = 0$ and $b_0 = -5$ mV/m the increase in c_0 is of ∼0.25 A/m and ∼0.2 A/m, larger than the current fed to the upward FAC region, which is not possible. This difficulty is cured for $b_0 = -10$ mV/m, where the increase in c_0 is just ∼0.12 A/m, while over the same time the integrated upward FAC is ∼0.02 A/m (see Fig. 5e). The sum of the two is roughly equal with the overall downward FAC, showing that from 8:29:00–8:29:15 the poleward current feeds both the EJ and the FAC.

With $b_0 = -10$ mV/m and given the abrupt decrease of the meridional electric field at 8:29:00, it is likely that from this time on the westward Pedersen component of the EJ is larger than the eastward Hall component — therefore around 8:29:00 the electrojet changes direction from eastward to westward. Thus, the current closure configuration from 8:29:00–8:29:15 is similar to the one from Event 1 just poleward of the CR. Later on, until 8:29:50, a decrease of about 0.15 A/m in the WEJ feeds about 0.07 A/m to the poleward current and about 0.08 A/m to the FAC, resulting in $j_\parallel \simeq 0.08$ A/m / 100 km = 0.8 μA/m^2. With $\Sigma_P \simeq 10$ mho and $E_\eta \simeq -10$ mV/m one obtains $J_{\eta_P} \simeq -0.1$ A/m and a variation length scale in J_{η_P} of 0.1 A/m / 0.8 μA/m^2 = 125 km, if the FAC is fed by the divergence of J_{η_P}. While this length scale is rather short, it is still 2.5 times larger than obtained for Event 1 (and, in view of the various error sources to be discussed next Section, it only provides a rough approximation). From 8:29:45 to the poleward boundary of the FAC, at 8:30:10, the poleward current feeds once more both the WEJ and the FAC.

In summary, for Event 2 the large scale downward and upward FACs are connected by meridional current and the electrojet is on average divergence free over each of these two regions. However, the smaller scale current closure remains rather complicated, similar in this sense to Event 1. Another similarity to Event 1 is the slightly negative value of the tangential electric field. However, unlike for Event 1, we believe that this time the FAC–EJ coupling is dominated by the Pedersen current driven by the tangential electric field.

3.3. Error sources

In the following we shall explore a number of possible error sources, that may result in false variations of the parameter c_0 and therefore false indications on the divergence of the electrojets. We identified six such error sources, to be addressed below: *(i)* errors in conductance; *(ii)* presence of neutral wind; *(iii)* errors in θ; *(iv)* arc curvature; *(v)* electric field inhomogeneous along η; *(vi)* temporal variations.

(i) Errors in conductance. The conductance estimates provided by Eqs. 7 and 8 are reliable only when the conductance is larger than a few mho. When the conductance is low, of the same order with the background level, the above equations are presumably not accurate. Because of this reason, we regard the results obtained for the upward FAC region to be in general more reliable, and in Section 4 we shall only concentrate on this region. Even here, time dependent variations of the conductance at the edges of the arc may still result in errors if the arc has a proper motion in the plasma system. However, according to *Haerendel et al.* [1993], such motions are quite slow, at speeds of ∼100 m/s or less, and the associated non-stationary behavior is likely to be confined to rather narrow regions, of a few km — with small effect on the results.

(ii) Presence of neutral wind. As discussed in Section 6.1 of M04, based on the statistical studies by *Brekke et al.* [1994] and *Nozawa and Brekke* [1995], the neutral winds around 21 MLT are likely to oppose the corotation. The associated small equatorward correction of the electric field can result in a change of the CR location equatorward, if the poleward field south of the CR is small as well. This is the case in Event 2, where the neutral wind correction may contribute to a partial decoupling of the large scale downward and upward FACs. Like for Event 1, this would add an overall positive EEJ divergence over the downward FAC and an overall negative WEJ divergence over the upward FAC.

(iii) Errors in θ. An error $\delta\theta$ in θ makes a false contribution of $H_y(1 - \cos\delta\theta)$ to the current closure normal to the arc. As long as $\delta\theta \leq 25°$, $1 - \cos\delta\theta < 0.1$, therefore one can tolerate relatively large errors in the inferred inclination of the current sheets. The errors in θ may also have a second effect, if the longitudinal displacement $\Delta\eta$ becomes large and c_0 can no longer be assumed as constant. However, for our two events both effects appear to be negligible. By using $\tan\theta = 0$, instead of $\tan\theta = 0.13$ for Event 1 and $\tan\theta = 0.26$ for Event 2, no significant changes of the results are observed.

(iv) Arc curvature. If the arc is folded, the cartesian geometry is no longer appropriate, and the arc curvature should be taken into account. By writing the current closure equation in polar coordinates, Eq. (4) transforms into:

$$j_\parallel - \frac{\partial J_\xi}{\partial \xi} = \frac{\partial J_\eta}{\partial \eta} + \frac{J_\eta}{R_\eta} = c_1 + \frac{J_\eta}{R_\eta} \qquad (12)$$

where ξ and η are the radial and tangential directions, respectively, while R_η is the radius of the arc. The term associated with the arc curvature, J_η/R_η, adds to the electrojet divergence, and can be significant if R_η is small enough. For example, if $J_\eta = 0.5$ A/m and $R_\eta = 500$ km, by working in cartesian coordinates one would obtain a false electrojet divergence of 1 μA/m^2. During relatively quiet times, auroral arcs are expected to be more or less aligned with magnetic latitude circles, whose radii in the auroral region are of the order of 2000 km, therefore arc curvature should not play a major role. However, actual arc radii can be influenced by small perturbations in the auroral current circuit, and small scale folds can be important in particular cases. The general conditions and the optical data suggest this is not the

case for our events, however, we cannot fully exclude such a possibility.

(v) Electric field inhomogeneous along η. If the electric field varies along η, according to Faraday's law b_0 should vary along ξ. Such variations can be significant in the upward FAC region, where the conductance is large, for example if $\Sigma_H = 20$ mho and $\delta b_0 = 5$ mV/m, then $\delta J_{\xi_H} = 0.1$ A/m. However, Figs. 4c and 6c suggest that in our events a certain amount of electric field inhomogeneity along η would not make a dramatic difference in the results. If b_0 were not constant, the actual c_0 profile would be bounded by the lines corresponding to the minimum and maximum values of b_0. Provided that δb_0 is rather small, the variation of the actual c_0 will still preserve the essential features discussed for the two events.

(vi) Temporal variations. If the aurora varies on time scales comparable with the width of the ALADYN sliding window, namely 10–20 s, temporal variations can introduce significant errors in the results. However, when the aurora changes on time scales longer than 1 min, as in our two events, temporal effects are presumably of minor importance. A check of $\Delta E_x/\Delta B_y$ supports this presumption, indicating in our case values much smaller than the Alfvén velocity (and comparable to $1/\mu_0\Sigma_P$) at fequencies of 50–100 mHz and below. The higher frequency Alfvénic activity between the ionosphere and the bottom side of the auroral acceleration region can also result in a mismatch between the data measured on FAST and the actual ionospheric values. However, this mismatch is smoothed out by ALADYN, since its time scale is significantly shorter than the duration of the ALADYN window.

While the combined effect of the errors analyzed above can contribute a significant fraction of the variation in c_0 and resulting divergence of the electrojets, we believe that this is more likely to happen for the quiet Event 2. For the growth phase Event 1, the large scale configuration, with the CR and FR boundaries close to each other, provides a strong indication that the inferred divergence of the electrojets is real.

4. M–I coupling implications of the ionospheric current closure

The divergence of the auroral electrojets is not surprising in itself and natural in certain regions — like the HR, where both the EEJ and WEJ terminate. The relevant question with respect to M–I coupling is whether field-aligned and electrojet currents are coupled to each other, that is, to what extent the electrojet divergence feeds or is fed by field-aligned currents. A divergent electrojet does not necessarily imply FAC–EJ coupling. For example, as shown already by *Kamide* [1978], during quiet times the FAC can be weak or missing in the HR, and the electrojets just couple to each other by meridional ionospheric currents.

Below we shall concentrate on the case with electric field uniform in longitudinal direction, and electrojet divergence driven by variations in the conductance. Since this is the model assumed by ALADYN, it is important to check that the results obtained are self-consistent. Our analysis will only cover the upward FAC, where the electron precipitation dominates and the higher conductance is more reliable. Assuming that the polarization is small, we shall first check the relative contributions of the Pedersen and Hall currents to the divergence of the electrojet, and further to the FAC–EJ coupling, depending on electron energy (and implicitly on the activity level). We shall then integrate the findings with recent results by *Amm et al.* [2011] and *Fujii et al.* [2011] regarding the Cowling mechanism, and suggest a tentative scenario for the auroral arc during the substorm cycle. In retrospect, we shall also check the assumption of small polarization and identify substorm stages when it is plausible that this assumption is fulfilled.

4.1. Pedersen and Hall contributions to the FAC–EJ coupling assuming small polarization

As demonstrated by Fig. 11a in M09, for electron energies above some 5 keV, the divergence of the electrojet relies on the variation of J_{η_H} — provided that the assumption of an electric field uniform in longitudinal direction holds. While this variation can still be compensated by the variation in J_{ξ_H}, rendering the Hall current divergence free, the Hall current *should* be coupled to the FAC when there is evidence for the FAC–EJ coupling. One notes that this feature is prominent only at higher electron energies, likely to be associated with auroral activity, and further with non-steady states of the auroral current circuit. As discussed in the next Section, in such cases a certain amount of the FAC carried Poynting flux can escape the dissipation in the ionosphere and feed back to the magnetospheric generator regions, contributing thus to the auroral reconfiguration. The possible FAC coupling with the Hall current appears thus to be consistent with higher electron energies and auroral activity.

The electrojet divergence and, possibly, FAC–EJ coupling at lower electron energies, as expected for rather quiet events, can be explored based on Fig. 7. The left panel is a zoom on the low energy end, 1–5 keV, of Fig. 11a from M09, showing the Pedersen and Hall components of the electrojet current, while the right panel is similar, but for the meridional current. It is assumed that in both longitudinal and meridional direction the field aligned current is uniform, leaving the electron average energy the only free parameter to control the induced conductance. While the assumption of FAC uniformity in longitudinal direction is related to the arc geometry, the uniformity in meridional direction is suggested by the often smooth profile of ΔB_y (and ΔB_x, when $\theta \neq 0$). In such cases, the variations of the field aligned current, $j_\parallel$, as indicated by the changes in the slope of ΔB_y, are smaller than the variations in conductance, motivating the assumption that electron energy has the dominant influence on the conductance profile (this is the case for Event 1 and Event 2).

Following M09, if $j_\parallel$ and, consequently, the number flux, Φ_N, are assumed to be constant, the energy flux, Φ_E, scales with the average energy, $\Phi_E = \overline{E}\Phi_N$, and the Pedersen and Hall conductance induced by electron precipitation, Eqs. (7), become:

$$\begin{aligned} \Sigma_P^e &= \frac{40\overline{E}^{1.5}}{16+\overline{E}^2}\Phi_N^{1/2} \\ \Sigma_H^e &= \frac{18\overline{E}^{2.35}}{16+\overline{E}^2}\Phi_N^{1/2} \end{aligned} \tag{13}$$

If the orientation of the electric field, E_η/E_ξ, is known, the Pedersen and Hall components of J_ξ and J_η have the following absolute values:

$$\begin{aligned} |J_{\xi P}| &= \Sigma_P|E_\xi| \\ |J_{\xi H}| &= \Sigma_H|E_\xi||E_\eta/E_\xi| \\ |J_{\eta P}| &= \Sigma_P|E_\xi||E_\eta/E_\xi| \\ |J_{\eta H}| &= \Sigma_H|E_\xi| \end{aligned} \tag{14}$$

Assuming, in addition, that the polarization effect, associated with the electric field divergence, $dE_\xi/d\xi$, is small, the relative contributions of the current components to the current closure can be read directly in Fig. 7. The lines there, indicating the variation of the respective current components with $\overline{E}$, are obtained based on Eqs. (13) and (14),

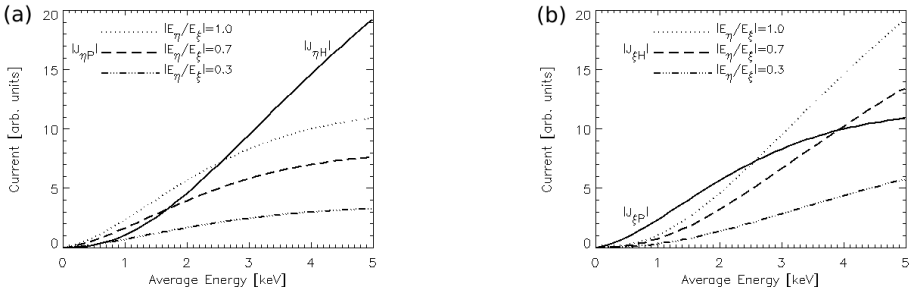

Figure 7. The relative contributions of the Pedersen and Hall components to the longitudinal (left) and meridional (right) current, depending on electron energy. It is assumed that the FAC (and number flux) is homogeneous in both directions, therefore the relative intensity of the currents $J_{\xi P}$, $J_{\xi H}$, $J_{\eta P}$, and $J_{\eta H}$ depends only on electron energy and on the ratio E_η/E_ξ. The plots show the absolute values of the electric field and current.

after dropping the common factors $\Phi_N^{1/2}$ and $|E_\xi|$. The small effect of the polarization, $dE_\xi/d\xi$, is a key assumption, expected to be fulfilled during quiet conditions (when the Hall current is likely to be divergence free), perhaps also during the growth phase and at the substorm onset. This issue will be discussed further in the next Section.

Figure 7 makes clear that at low energies the variation of the Hall component of the electrojet is comparable with the variation of the Pedersen component, with the exact ratio depending on the the orientation of the electric field, E_η/E_ξ. Moreover, the variation of $J_{\eta H}$ can be equal to the variation of $J_{\xi H}$ but of opposite sign, rendering thus the divergence of the vector Hall current equal to zero — as expected during steady state, quiet conditions.

The discussion on the conductance variation and on the divergence of the Hall current can be extended by considering the variation length scales of $\overline{E}$ in both ξ and η. A zero divergence of the Hall current implies that $|\partial J_{\xi_H}/\partial\xi| = |\partial J_{\eta_H}/\partial\eta|$, which can be processed to yield:

$$\frac{\lambda_\xi^{\overline{E}}}{\lambda_\eta^{\overline{E}}} = \left|\frac{E_\eta}{E_\xi}\right| \tag{15}$$

provided that the assumptions of constant electric field and uniform FAC are reasonable. The partial derivatives were replaced by means of the variation length scales of the electron energy, $\partial/\partial(\xi,\eta) \simeq 1/\lambda_{\xi,\eta}^{\overline{E}}$. (The reader is cautioned against possible confusion between the electric field components, E_ξ, E_η, and the average energy, $\overline{E}$).

If the tangential electric field is much smaller than the normal electric field, $E_\eta \ll E_\xi$, as expected in the evening and morning sectors, Eq. 15 shows that for steady state quiet arcs the longitudinal length scale is much larger than the meridional one — consistent with the quiet arc geometry. Small scale perturbations in the magnetosphere, that drive locally the M–I system out of the steady state, could result in local violations of Eq. (15). Such perturbations could be related e. g. to bursty bulk flows, and map to auroral streamers or polar boundary intensifications in the ionosphere [e. g. *Henderson et al.*, 1998; *Lyons et al.*, 1999].

When the tangential electric field is significant, as expected in the Harang region, Eq. (15) suggests that steady state arcs should be less elongated. Alternatively, one can interpret Eq. (15) in the sense that a mismatch is more likely, and therefore the Hall current is more likely to be coupled with the FAC. This interpretation is in good agreement with the dynamic character of the HR, where non-steady states are more likely to occur.

4.2. The auroral arc during the substorm cycle — a tentative scenario

In a recent statistical study based on radar and ground magnetic field data, *Amm et al.* [2011] obtained indirect evidence that the Cowling efficiency is likely to increase with substorm intensity (their Fig. 6b). The Cowling efficiency, α_C, can vary between 0 and 1 and is defined by:

$$\nabla \cdot \mathbf{J}_{P_2} = -\alpha_C \nabla \cdot \mathbf{J}_H \tag{16}$$

where $\mathbf{J}_{P_2}$ is the Pedersen current driven by the secondary electric fields due to polarization charges. When $\alpha_C = 0$ / $\alpha_C = 1$ the Hall current is fully coupled to the FAC / polarization Pedersen current. *Amm et al.* [2011] found that the Cowling efficiency is likely to approach zero at quiet (and weakly disturbed) times, which means that the polarization charge vanishes, $\nabla\cdot\mathbf{J}_{P_2} \simeq 0$. Since at quiet times the FAC is not expected to couple to the Hall current, the appropriate interpretation of this results is that $\nabla \cdot \mathbf{J}_H \simeq 0$.

When the auroral activity, as measured by the electrojet index, increases, a certain amount of FAC coupling to the Hall current can occur, depending on α_C. According to *Fujii et al.* [2011] (their Fig. 4), the larger α_C is, the more substantial is the fraction of the FAC carried Poynting flux that feeds Joule heating associated with polarization Pedersen currents. An intriguing question raised by Fig. 4 of *Fujii et al.* [2011] is that when $\alpha_C = 1$ the Hall current is entirely closed by polarization Pedersen currents and fully decoupled from the FAC. While a detailed consideration of this question is beyond the scope of the present paper, we note that the time dependent character of the FAC coupling to the Hall current is likely to play an important role. In a time dependent configuration one can imagine e.g. a two-step process, first some inductive accumulation of the energy fed by the Hall coupled FAC, followed at a later stage by resistive dissipation via secondary Pedersen currents. If $\alpha_C = 1$, at this stage the FAC is no longer coupled to the Hall current.

The evolution of the ionospheric current closure during the substorm cycle can be integrated with the evolution of the Cowling mechanism in the following tentative scenario. A prime target for this scenario, formulated for the time being in qualitative terms, is the auroral arc.

1. At quiet times the Hall current is likely to be divergence free, the polarization is negligible, and the FAC is closed by Pedersen currents. In the evening and morning sector the Pedersen current is normal to the arc, while in the Harang region the FAC–EJ coupling can be achieved in a mixed 'Type 1/Type 2' configuration. The FAC sheet (Type 1) is azimuthally connected to the Pedersen component of the EJ (Type 2), driven by the westward component of the electric field. This could be the case for our quiet Event 2.

2. As soon as the substorm starts to grow, a small amount of Hall current divergence becomes available to couple with the FAC and a fraction of the Poynting flux carried by the Hall coupled FAC may be stored inductively, contributing to

a gradual enhancement of the electrojet current system and a slow change of the auroral current circuit. The FAC–EJ coupling can thus be partially achieved based on the Hall current. The polarization is small, if at all. This could be the case for our growth phase Event 1.

3. At onset and shortly afterwards, when the M–I system is far from equilibrium, most of the Hall current divergence may couple with the FAC. Consequently, the Cowling efficiency and the polarization are low, and the FAC–EJ coupling can be dominated by Hall currents. At this stage, the sudden break of equilibrium between magnetosphere and ionosphere triggers also Alfvén waves, bouncing back and forth along auroral flux tubes becasue of the missmatch between the wave admittance, Σ_A, the ionospheric conductance, Σ_P, and the effective conductance of the magnetospheric generator, Σ_G [*Lysak*, 1986].

4. Later on during the expansion phase, when some sort of dynamic equilibrium is achieved, the Cowling channel can become fully developed and the divergence of the Hall current feeds the secondary Pedersen currents. The polarization plays now a major role. The FAC closure is achieved by the primary Pedersen currents. As pointed out above, the energy transfer to the ionospheric circuit that includes the divergent part of the Hall current and the secondary Pedersen current requires further examination.

5. During the recovery phase, the M–I system reapproaches an equilibrium state, therefore the FAC coupling to the Hall current is likely to be less important. The Cowling efficiency may remain high but with less and less Hall current divergence to feed polarization Pedersen currents. The energy stored inductively during the growth phase is dissipated and the current system gets back to quiet time parameters. Eventually, the Hall current divergence gets back to zero and the Cowling channel dies out.

Before concluding this Section, one should emphasize the difference between the two unsteady behaviors of the auroral M–I system mentioned above. On one hand, the examination of the dynamic auroral flux tube and the bouncing Alfvén waves was typically done by assuming the FAC coupling to Pedersen currents and a divergence free Hall current [e. g. *Lysak*, 1986]. The time scale of reaching the equilibrium is of the order of minutes, corresponding to a few Alfvén bounces — with the exact number depending on the specific parameters of the magnetospheric generator, of the ionospheric load, and along the flux tube. On the other hand, the FAC coupling to Hall currents received comparatively much less attention, possibly because such a coupling is difficult to envisage under steady state conditions. In this case, the time scale should be related to the rise and fall of the electrojet current system, presumably shorter for a local activation and longer for a fully developed substorm. This matter requires further investigation, which is, however, beyond the scope of this paper.

5. Summary

The results of this paper can be summarized as follows:

1. The ALADYN technique was updated and allows now the exploration of the data on a continuous time basis, providing approximate profiles of the electrojet divergence along the satellite ionospheric footpoint. The tangential electric field can also be inferred within a certain range.

2. In order to validate the updates, ALADYN was applied first to an event studied before, FAST Orbit 1859, located in the Harang region. The new results were found to be in good agreement with the old conclusion that in this case both the EEJ and the WEJ are divergent and coupled to the downward and upward FAC, respectively.

3. The updated ALADYN was then used to investigate a quiet event in the evening sector, FAST Orbit 1805. This investigation suggests that the electrojet divergence can still be significant over certain latitudinal ranges, a finding that does not fit with the 1D model of the evening auroral arc. However, because of the various error sources, this result should be treated with care. More event studies are needed, ideally with conjugate optical data, as well as ground radar and magnetic field data.

4. The examination of the local current closure suggests that at certain locations the electrojet divergence feeds the FAC. The FAC–EJ coupling was identified for both events, but it was found to be more prominent for FAST orbit 1859, where the close proximity of the convection reversal and FAC reversal boundaries prevents the standard connection between the downward and upward FAC sheets. The FAC–EJ coupling is likely to be achieved mainly by Pedersen current, driven by the tangential electric field, for the quiet Event 2, while for the slightly more disturbed Event 1 the Hall closure appears to be significant as well.

5. The examination of the current closure depending on electron energies, confirmed that at low energies the Hall current is likely to be divergence free, while at higher energies, associated with active aurora, the FAC–EJ coupling relies on the Hall current. Important assumptions underlying this result are the longitudinal homogeneity of the electric field and field-aligned current, as well as the neglect of the ionospheric polarization. In order to check the longitudinal homogeneity, two measuring points at neighboring MLTs are required, a setup to be provided systematically by the upcoming Swarm mission.

6. In agreement with M09, but based this time on a scale argument, we showed that the FAC coupling to the Hall current is more likely in the Harang region, where the tangential electric field is typically larger. The FAC coupling to the Hall current is consistent with the more dynamic character of the Harang region. In general, the actual auroral configuration varies from event to event and, even during quiet periods, small scale perturbations in the magnetosphere can induce reconfigurations of the auroral current circuit — with impact on the ionospheric current closure.

7. The findings of the paper were integrated with recently published results on the Cowling mechanism in a qualitative scenario that describes, tentatively, the evolution of the auroral arc during the substorm cycle. The unsteadiness of the auroral flux tube due to bouncing Alfvén waves, which does not require a divergent Hall current, was contrasted with the rise and fall of the electrojet current system, associated presumably with FAC coupling to the Hall current. More experimental evidence and theoretical work are needed to validate this scenario.

Acknowledgments. A preliminary version of this paper was presented at the Auroral Plasma Physics Workshop held in Beaulieu, France, in May 2010. We thank Jim McFadden, Bob Strangeway, Hans Nilsson, Joachim Vogt, and Jesper Gjerloev for helpful comments. The final form of the paper benefited from fruitful discussions within the POLARIS team at ISSI. The work at ISS Bucharest was supported by the project ECSTRA, ESA Contract 4200098048, carried on under the PECS programme.

References

Amm, O., P. Janhunen, H. Opgenoorth, T. Pulkkinen, and A. Viljanen, Ionospheric shear flow situations observed by the MIRACLE network and the concept of Harang discontinuity, in *Magnetospheric current systems*, edited by S. Ohtani, R. Fujii, M. Hesse, and R. Lysak, no. 118 in Geophysical Monograph, pp. 227–236, AGU, Washington, D.C., 2000.

Amm, O., R.Fujii, K. Kauristie, A. Aikio, A. Yoshikawa, A. Ieda, and H. Vanhamamäki, A statistical investigation of the Cowling channel efficiency in the auroral zone, *J. Geophys. Res.*, *116*, A02,304, doi:10.1029/2010JA015,988, 2011.

Baumjohann, W., Ionospheric and field-aligned current systems in the auroral zone: A concise review, *Adv. Space Res.*, *2*(10), 55–62, 1982.

Boström, R., A model of the auroral electrojets, *J. Geophys. Res.*, *69*, 4983–4999, 1964.

Brekke, A., S. Nozawa, and T. Sparr, Studies of the *E* region neutral wind in the quiet auroral ionosphere, *J. Geophys. Res.*, *99*, 8801–8825, 1994.

de la Beaujardière, O., R. Vondrak, and M. Baron, Radar observations of electric fields and currents associated with auroral arcs, *J. Geophys. Res.*, *82*, 5051–5062, 1977.

Fujii, R., O. Amm, A. Yoshikawa, A. Ieda, and H. Vanhamamäki, Reformulation and energy flow of the Cowling channel, *J. Geophys. Res.*, *116*, A02,305, doi:10.1029/2010JA015,989, 2011.

Galand, M., and A. Richmond, Ionospheric electrical conductances produced by auroral proton precipitation, *J. Geophys. Res.*, *106*, 117–125, 2001.

Haerendel, G., S. Buchert, C. La Hoz, B. Raaf, and E. Rieger, On the proper motion of auroral arcs, *J. Geophys. Res.*, *98*, 6087–6099, 1993.

Henderson, M., G. Reeves, and J. Murphree, Are northsouth structures an ionospheric manifestation of bursty bulk flows?, *Geophys. Res. Lett.*, *25*, 3737–3740, 1998.

Iijima, T., and T. Potemra, The amplitude distribution of field-aligned currents at northern high latitudes observed by Triad, *J. Geophys. Res.*, *81*, 2165–2174, 1976.

Kamide, Y., On current continuity at the Harang discontinuity, *Planet. Space Sci.*, *26*, 237–244, 1978.

Lyons, L., T. Nagai, G. Blanchard, J. Samson, T. Yamamoto, T. Mukai, A. Nishida, and S. Kokubun, Association between geotail plasma flow and auroral poleward boundary intensifications observed by CANOPUS photometers, *J. Geophys. Res.*, *104*, 4485–4500, 1999.

Lysak, R., Coupling of the dynamic ionosphere to auroral flux tubes, *J. Geophys. Res.*, *91*, 7047–7056, 1986.

Marghitu, O., B. Klecker, G. Haerendel, and J. McFadden, ALADYN: A method to investigate auroral arc electrodynamics from satellite data, *J. Geophys. Res.*, *109*, A11,305, doi:10.1029/2004JA010,474, 2004.

Marghitu, O., T.Karlsson, B. Klecker, G. Haerendel, and J. McFadden, Auroral arc and oval electrodynamics in the Harang region, *J. Geophys. Res.*, *114*, A03,214, doi:10.1029/2008JA013,630, 2009.

Marklund, G., Auroral arc classification scheme based on the observed arc-associated electric field pattern, *Planet. Space Sci.*, *32*, 193–211, 1984.

Nielsen, E., and R. Greenwald, Electron flow and visual aurora at the Harang discontinuity, *J. Geophys. Res.*, *84*, 4189–4200, 1979.

Nozawa, S., and A. Brekke, Studies of the *E* region neutral wind in the disturbed auroral ionosphere, *J. Geophys. Res.*, *100*, 14,717–14,734, 1995.

Robinson, R., R. Vondrak, K. Miller, T. Dabbs, and D. Hardy, On calculating ionospheric conductances from the flux and energy of precipitating electrons, *J. Geophys. Res.*, *92*, 2565–2569, 1987.

Stenbaek-Nielsen, H., T. Hallinan, D. Osborne, J. Kimball, C. Chaston, J. McFadden, G. Delory, M. Temerin, and C. Carlson, Aircraft observations conjugate to FAST: Auroral arc thicknesses, *Geophys. Res. Lett.*, *25*, 2073–2076, 1998.

Sugiura, M., A fundamental magnetosphere-ionosphere coupling mode involving field-aligned currents as deduced from DE-2 observations, *Geophys. Res. Lett.*, *11*, 877–880, 1984.

Weygand, J., R. McPherron, H. Frey, O. Amm, K. Kauristie, A. Viljanen, and A. Koistinen, Relation of substorm onset to Harang discontinuity, *J. Geophys. Res.*, *113*, A04,213, doi:10.1029/2007JA012,537, 2008.

Zou, S., L. Lyons, C.-P. Wang, A. Boudouridis, J. Ruohoniemi, P. Anderson, P. Dyson, and J. Devlin, On the coupling between the Harang reversal evolution and substorm dynamics: A synthesis of SuperDARN, DMSP, and IMAGE observations, *J. Geophys. Res.*, *114*, A01,205, doi:10.1029/2008JA013,449, 2009.

C. Bunescu, Institute for Space Sciences, P.O.Box MG-23, RO-77125 Bucharest-Măgurele, Romania

T. Karlsson, Space and Plasma Physics, School of Electrical Engineering, Royal Institute of Technology, S-10044 Stockholm, Sweden

B. Klecker, Max Planck Institute for Extraterrestrial Physics, D-85748 Garching, Germany

O. Marghitu, Institute for Space Sciences, P.O.Box MG-23, RO-77125 Bucharest-Măgurele, Romania
(marghitu@gpsm.spacescience.ro)

H.C. Stenbaek-Nielsen, University of Alaska at Fairbanks, Fairbanks, Alaska 99775, USA